



GAS-PHASE ABSORPTIONS OF C_{60}^+ : A NEW COMPARISON WITH ASTRONOMICAL MEASUREMENTS^{*†}

G. A. H. WALKER¹, E. K. CAMPBELL², J. P. MAIER², D. BOHLENDER³, AND L. MALO⁴

¹1234 Hewlett Place, Victoria, BC V8S 4P7, Canada; gordonwa@uvic.ca

²Department of Chemistry, University of Basel, CH-4056 Basel, Switzerland; ewen.campbell@unibas.ch, j.p.maier@unibas.ch

³National Research Council of Canada, Herzberg Astronomy and Astrophysics; 5071 West Saanich Road,
Victoria, BC V9E 2E7, Canada; david.bohlender@nrc-cnrc.gc.ca

⁴CFHT Corporation, Kamuela, Hawaii 96743, USA; malo@cfht.hawaii.edu

Received 2016 July 21; revised 2016 August 4; accepted 2016 August 5; published 2016 November 3

ABSTRACT

Campbell et al. recently revised, by a few tenths of an Å, the wavelengths for their low-temperature laboratory measurements of fullerene C_{60}^+ bands. This accounts for the perturbation caused by the He atom to the C_{60}^+ -He spectrum. Here, we demonstrate that the revised laboratory wavelengths improve coincidence with the 9632, 9577, 9428, 9365, and 9348 diffuse interstellar bands detected towards the stars HD 46711, HD 169454, and HD 183143.

Key words: ISM: molecules

1. INTRODUCTION

The assignment of five diffuse interstellar bands (DIBs) to absorption by the cation C_{60}^+ from gas-phase laboratory measurements below 10 K (Campbell et al. 2015, 2016a; Walker et al. 2015) is the first robust assignment of a DIB carrier. The widths (~ 2.5 Å) of the laboratory bands of C_{60}^+ come from internal conversion. This follows the first observation of the 9577 and 9632 DIBs by Foing and Ehrenfreund (1994) and their suggestion, based on the matrix spectrum (Fulara et al. 1993), that these are due to C_{60}^+ . Subsequent studies confirmed these two bands to be interstellar (for references see Cox et al. 2014).

In the laboratory, the spectrum actually measured was of the complex C_{60}^+ -He. It was recognized that, although the He atom is weakly bound, it does introduce errors to the wavelengths of bare C_{60}^+ (Campbell et al. 2016a). There also appears to be a systematic offset between the laboratory and astronomical wavelengths of a few tenths of an Å for the two reddened stars, HD 183143 and HD 169454, considered by Walker et al. (2015).

Campbell et al. (2016b) have now estimated the perturbation caused by the He atom from the linear change in wavelength of the origin bands of C_{60}^+ -He_{*n*} (*n* = 1–3), allowing extrapolation to *n* = 0, with a residual uncertainty of ~ 0.2 Å in the wavelengths for bare C_{60}^+ .

In this paper we demonstrate agreement of the revised C_{60}^+ laboratory wavelengths 9632.1, 9577.0, 9427.8, 9365.2, and 9348.4 Å (Campbell et al. 2016b) with the 9632, 9577, 9428, 9365, and 9348 DIBs towards the reddened stars HD 46711, HD 169454, and HD 183143.

2. ASTRONOMICAL OBSERVATIONS

Spectra of the heavily reddened B stars HD 183143, HD 169454, and HD 46711 were taken using the CFHT ESPaDOnS spectrograph (Donati 2003) fiber-fed from the CFH 3.6 m telescope (for HD 183143 and HD 169454) and using GRACES⁵ (Chené et al. 2014) from the 8 m Gemini-North telescope (for HD 46711). The ESPaDOnS spectral resolution is approximately 65,000 or 0.05 Å per pixel. A gap in spectral coverage between 9608 and 9636 Å, where the échelle order lies off the edge of the detector, prevents detection of the 9632 DIB. To study the 9632 DIB, we recovered the spectra of HD 183143 and the standards published by Foing & Ehrenfreund (1997; see their Figure 1), which were taken using the CFHT *f*/8.2 coude spectrograph at a resolution of $\sim 40,000$ in the first order. Details of the stars and their standards are given in Table 1.

Telluric water vapor (WV) lines seriously contaminated the region of the C_{60}^+ laboratory bands (see Figure 1 in Walker et al. 2015). These were eliminated to the first order by normalization with spectra taken at the same air mass of a rapidly rotating star where rotational line broadening was large enough to avoid confusion in DIB identification. An unreddened spectral standard matching as closely as possible the spectral type and luminosity class of the reddened target star was also observed to correct for weak stellar features for HD 46711 and HD 183143.

The ESPaDOnS spectra of HD 183143 and standards were taken on 2015 July 28 UT. The full details of the reductions are given in Walker et al. (2015). Spectra of HD 46711 were acquired on 2015 December 17 UT with ≤ 1 mm precipitable WV and within ± 1.5 hr of meridian crossing. The latter spectra were reduced using an adapted version of the OPERA reduction software under development at CFHT (Martoli et al. 2012) for the GRACES data (L. Malo 2016, in preparation). Data for HD 169454 were downloaded from the Canadian Astronomy Data Centre's CFHT archive. This star was observed on 2005 May 21.

^{*} Based on observations obtained at the Canada–France–Hawaii Telescope, which is operated by the National Research Council of Canada, the Institut National des Sciences de l'Univers of the Centre National de la Recherche Scientifique of France, and the University of Hawaii.

[†] Based on observations obtained at the Gemini Observatory, which is operated by the Association of Universities for Research in Astronomy, Inc., under a cooperative agreement with the NSF on behalf of the Gemini partnership: the National Science Foundation (United States), the National Research Council (Canada), CONICYT (Chile), Ministerio de Ciencia, Tecnología e Innovación Productiva (Argentina), and Ministério da Ciência, Tecnologia e Inovação (Brazil).

⁵ Gemini Remote Access to CFHT ESPaDOnS Spectrograph.

Table 1
ESPaDONs, GRACES, and CFHT *f*/8.2 Observations

Star	Sp/L	<i>I</i>	<i>V</i>	$E_{(B-V)}$	$\Delta\lambda_K$ Å	$\Delta\lambda_{9577}$ Å
HD 183143	B7 Ia	4.79	6.86	1.28	-0.30, +0.09	-0.37, +0.11
HR 7437	B8 III _n	5.10	5.00	0.00	...	(-0.15) ^a
Rigel	B8 Iae	0.15	0.13	0.00
HR 7235 ^b	A4 IV _{nn}	2.98	2.99	0.00
HD 169454	B1 Ia	5.13	6.71	1.12	-0.29	-0.36
HR 7235 ^b	A4 IV _{nn}	2.98	2.99	0.00
HD 46711	B3 II ^c	7.77	9.25	1.05	+0.67	+0.83
HD 49567	B2.5 III	...	6.15	0.00
HR 2395 ^b	B5V n	...	5.08	0.00

Notes.

^a Weighted mean for HD 183143 (see text).

^b $v \sin i \geq 300 \text{ km s}^{-1}$.

^c Spectral classification from Hiltner (1956) confirmed by our spectra.

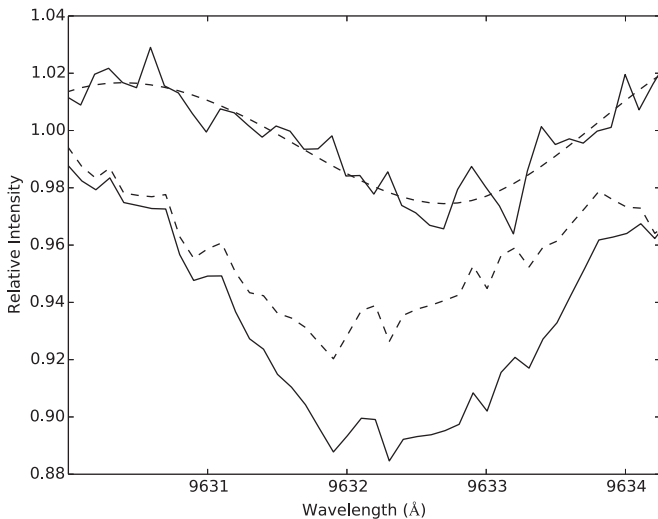


Figure 1. Top: profile of the 9632.1 Å Mg II stellar absorption feature fitted with a polynomial (dashed) in the Rigel spectrum, shifted in wavelength to match the radial velocity of HD 183143. Lower: profile of the 9632 DIB in the HD 183143 spectrum before and after (dashed line) subtraction of the polynomial.

The CFHT *f*/8.2 observations of HD 183143 and standards were made on 1995 March 21 UT with very low precipitable WV (<0.25 mm). The 9632 DIB coincides with a stellar absorption line of Mg II at 9632.1 Å in B-type spectra. Rigel closely matches HD 183143 in both spectral type and luminosity class but suffers no interstellar reddening. Foing & Ehrenfreund (1997) acquired spectra of Rigel at large air mass (2.7) on the same night, but since the 9632 DIB is not affected by strong WV lines, it could be used to correct for the Mg II stellar feature. We made a polynomial fit to the profile of the Rigel 9632.1 Å Mg II feature, as shown in Figure 1, after shifting the Rigel spectrum by -0.16 Å to compensate for the difference in radial velocity between Rigel and HD 183143. We then subtracted the polynomial from the HD 183143 9632 DIB. The pre- and post-deblending profiles are shown together in Figure 1.

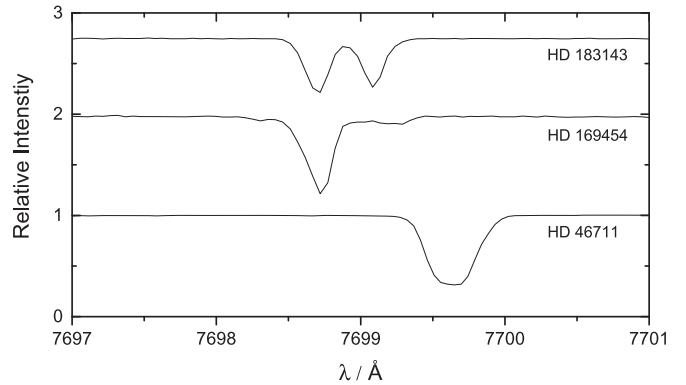


Figure 2. Profiles of the interstellar potassium lines for HD 183143, HD 169454, and HD 46711 after correction for telluric WV lines. The air wavelength assumed for the K line is 7699.0 Å.

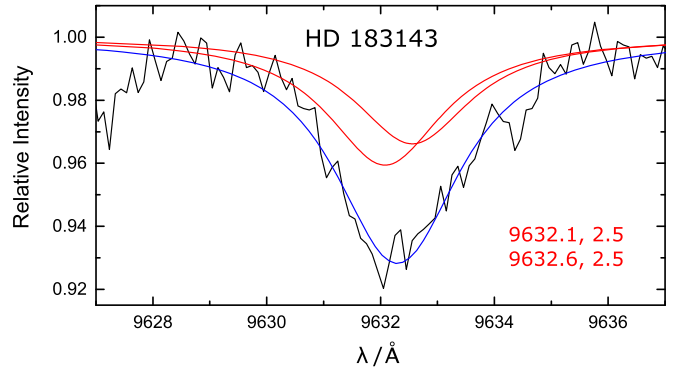


Figure 3. 9632 DIB in the spectrum of HD 183143 after elimination of the 9632.1 Å Mg II stellar line (see Figure 1) and correction for the average interstellar 7699.0 Å K line offset of -4.7 km s^{-1} . A two-cloud model is used, where the red lines are Lorentzian fits to the astronomical data and the blue line is the cumulative profile. The best fitting parameters are listed in red (λ , FWHM); they were constrained by the wavelengths and widths of the laboratory spectrum (see text for details).

2.1. The Interstellar Clouds and Their Radial Velocities

Figure 2 shows the spectral region of the interstellar K line at 7699.0 Å as observed for each star with ESPaDONs after removal of telluric WV lines. Only for HD 169454 is there evidence of a single absorbing cloud, in this case displaced by -0.29 Å or -11 km s^{-1} . In the case of HD 183143 there are two clouds separated by 0.39 Å or 15 km s^{-1} with an area ratio 1.2:1. The weighted average displacement of the two K lines is -0.12 Å or -4.7 km s^{-1} based on the area ratio. For HD 46711 the K line is significantly broadened ($\sim 1 \text{ Å}$) by two or more unresolved components. The displacements of the K line components in Å, $\Delta\lambda_K$, for each star are listed in Table 1 together with the values of $\Delta\lambda_{9577}$ derived from them. A mean is given for HD 46711. It should be noted that although wavelengths are quoted to one hundredth of an Å, the accuracy is closer to one tenth when all sources of error are taken into account.

2.2. DIB Characteristics

The profiles of the detected DIBs are plotted in Figures 3–7. The ESPaDONs spectra are all smoothed by a 5-pixel boxcar. The *f*/8.2 spectra are unsmoothed. A stellar emission line inhibited detection of the 9428 DIB for HD 183143 (Walker et al. 2015), and the quality of the archival HD 169454

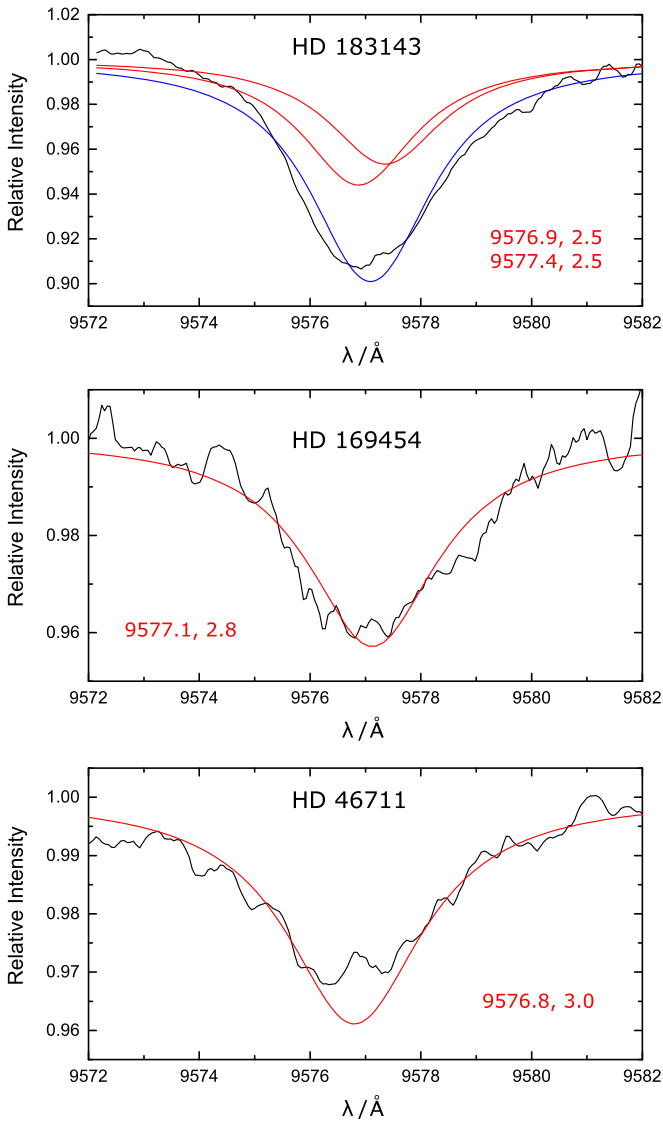


Figure 4. 9577 DIB in spectra of HD 183143, HD 169454, and HD 46711. The red lines are the Lorentzian fits to the astronomical data. The best fitting parameters are listed in red; they were constrained by the wavelengths and widths of the laboratory spectrum (see text for details). The HD 183143 fit uses a two-cloud model, and the blue line is the cumulative profile.

spectrum was inadequate for the identification of the weakest DIB, 9348. Apart from the 9632 DIB, the DIB profiles for HD 183143 and HD 169454 are identical to those published by Walker et al. (2015), except that the reflex of the velocity shifts derived from the values of $\Delta\lambda_K$ in Table 1 was applied for each star. For HD 183143 the weighted mean value, -4.7 km s^{-1} , was applied, in contrast to the case in Walker et al. (2015), where only the stronger K line component value was used.

HD 46711 was chosen as a target because it, together with HD 183143, has one of the strongest known 4428 DIB (Walker 1962). Clearly, however, the C_{60}^+ DIBs in HD 46711 have, at best, only one third the strength of those in HD 183143, which means that the carriers of the 4428 Å and C_{60}^+ bands cannot be the same. Despite the weakness of the C_{60}^+ DIBs in HD 46711, the 9348 DIB does appear to exist.

Unlike the 9632 and 9577 DIBs, the other three DIBs are very weak, generally being only a fraction of a percent. This

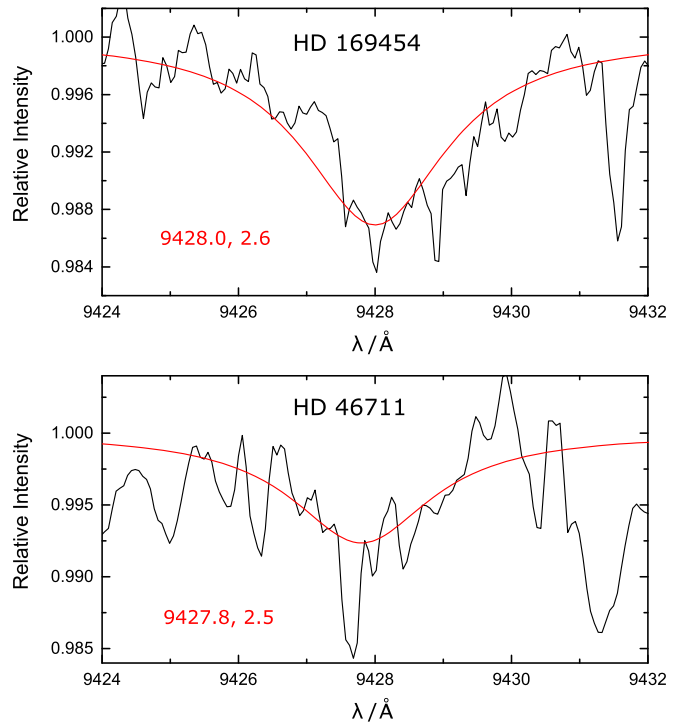


Figure 5. 9428 DIB in spectra of HD 169454 and HD 46711. The red lines are the Lorentzian fits to the astronomical data. The best fitting parameters are listed in red; they were constrained by the wavelengths and widths of the laboratory spectrum (see text for details). Large water vapor line residuals at 9427.5 and 9428.2 Å in the unshifted stellar spectra have been omitted and replaced by averages for both stars.

means that the profiles are sensitive to the process of WV elimination and the setting of the continua. Defining the profiles is further complicated by the presence of companion DIBs of similar strength and FWHM at 9351 and 9362 Å in the wings of the weakest DIBs, 9348 and 9365. It is interesting to note that the unassigned 9351 and 9362 DIBs are equally strong for both HD 183143 and HD 46711.

3. COMPARISON WITH THE LABORATORY DATA

Walker et al. (2015) fitted Gaussian curves to the HD 183143 and HD 169454 DIBs. Here, we fit Lorentzian functions to the DIB profiles in Figures 3–7. The fitting parameters were constrained by the laboratory wavelengths (Campbell et al. 2016b) and the characteristics of the K line(s) in Figure 2. The wavelengths were allowed to vary by up to $\pm 0.2 \text{ Å}$, reflecting the reported experimental uncertainty.

For HD 183143 there are two interstellar clouds. The corresponding K lines have an intensity ratio of 1.2:1 (Figure 2), and the wavelength offsets from 7699.0 Å are given in Table 1. The corresponding offsets in the spectral region of the DIBs are -0.37 and $+0.11 \text{ Å}$, and their weighted mean displacement is -0.15 Å . To account for the contribution from both clouds, each of the DIBs observed toward HD 183143 was fit using two Lorentzian profiles. The central wavelengths of the latter were displaced from the laboratory values by the difference from the weighted mean (-0.22 and $+0.26 \text{ Å}$). The area ratio of 1.2:1 and the 0.48 Å separation in the central wavelength were fixed. The values of the FWHM were allowed to vary between 2.1 and 2.5 Å, corresponding to the range observed in the laboratory spectra.

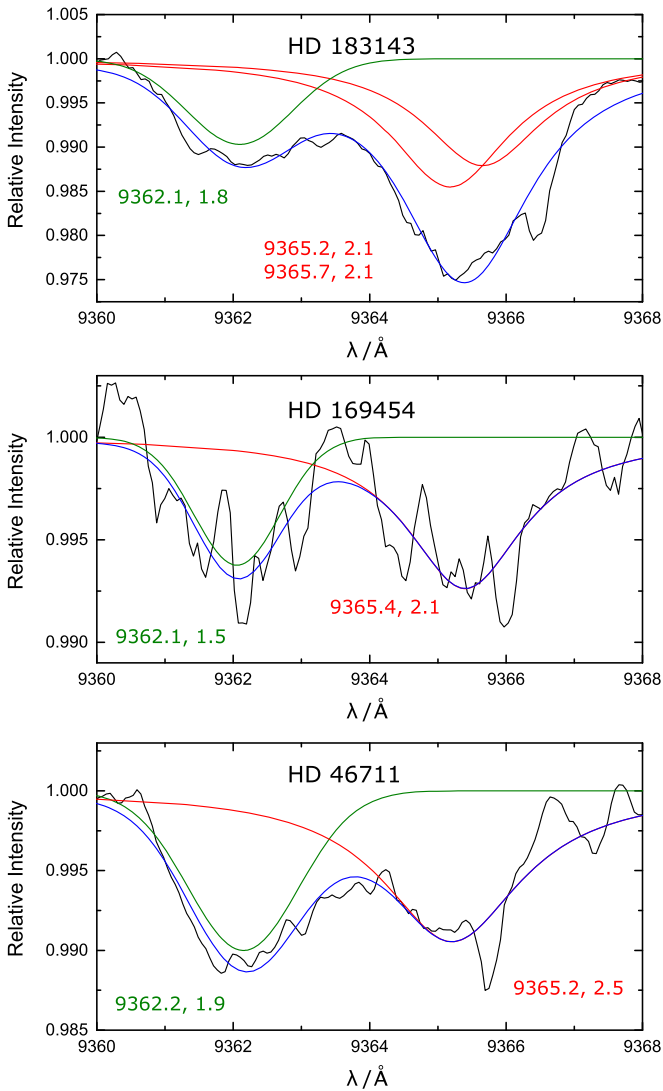


Figure 6. 9365 DIB in spectra of HD 183143, HD 169454, and HD 46711. The red lines are the Lorentzian fits to the astronomical data. The best fitting parameters are listed in red; they were constrained by the wavelengths and widths of the laboratory spectrum (see text for details). The HD 183143 fit uses a two-cloud model. The green lines are the Gaussian fits (parameters in green) to the unassigned DIB (~ 9362 Å), and the blue lines are the cumulative profiles.

Only a single K line is seen in the spectrum of HD 169454, and the observed DIBs were fitted with a single Lorentzian function. The best fits were obtained by relaxing the FWHM constraint and allowing values up to 3 Å. The K line observed in the spectrum of HD 46711 is broader than those of both HD 183143 and HD 169454, suggesting two or more unresolved components.

The 9632, 9577, 9428, 9365, and 9348 DIBs and Lorentzian fits are presented in Figures 3–7, together with the values of the best fitting central wavelengths and FWHMs. The profiles of the unassigned DIBs at 9351 and 9362 Å were fitted with Gaussians, and the values of the central wavelength and FWHM are also given in the figures. Due to the weakness of the 9428 and 9348 DIBs observed in the spectrum of HD 46711, additional constraints were applied to the fitting parameters to obtain the results presented in Figures 5 and 7. In

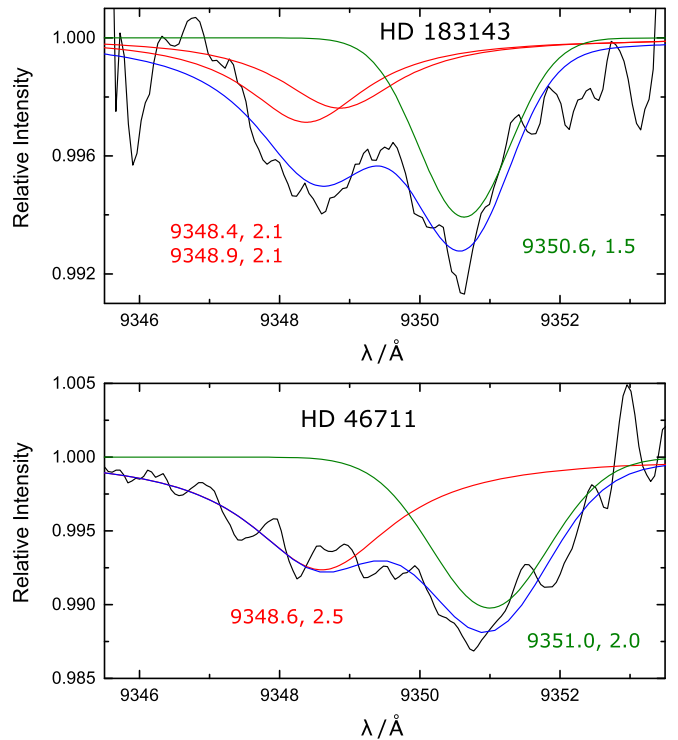


Figure 7. 9348 DIB in spectra of HD 183143 and HD 46711. The red lines are the Lorentzian fits to the astronomical data. The best fitting parameters are listed in red; they were constrained by the wavelengths and widths of the laboratory spectrum (see text for details). The HD 183143 fit uses a two-cloud model. The green lines are the Gaussian fits (parameters in green) to the unassigned DIB (~ 9351 Å), and the blue lines are the cumulative profiles.

both cases the FWHM was fixed at 2.5 Å, while for the former fit, the central wavelength was set at 9427.8 Å.

Agreement between the laboratory C_{60}^+ absorptions and the DIBs detected toward HD 183143 is clear without the need to assume that one of the two clouds sampled along the line of sight makes a dominant contribution. In addition, the deblending of the 9632 DIB leads to an intensity ratio of 1:0.7 for the 9577 and 9632 DIBs, which is close to that observed in the laboratory (Campbell et al. 2016a). Although the C_{60}^+ bands are weaker for HD 46711, the 9577, 9428, 9365, and 9348 DIBs are all present, and agreement with the laboratory profiles is convincing. This detailed comparison now consolidates the agreement of five absorption bands of C_{60}^+ with DIBs observed in the spectra of several reddened stars.

The observations of HD 46711 were carried out under the Gemini Fast Turnaround program FT-19. The assistance of Dr. André-Nicolas Chené and Dr. Andreea Petric is gratefully acknowledged. This research used the facilities of the Canadian Astronomy Data Centre, operated by the National Research Council of Canada with the support of the Canadian Space Agency.

REFERENCES

- Campbell, E. K., Holz, M., Gerlich, D., & Maier, J. P. 2015, *Natur*, **523**, 322
 Campbell, E. K., Holz, M., Maier, J. P., et al. 2016a, *ApJ*, **822**, 17
 Campbell, E. K., Holz, M., & Maier, J. P. 2016b, *ApJL*, **826**, L4
 Chené, A.-N., Padzer, J., Barrick, G., et al. 2014, *Proc. SPIE*, **9151**, 47
 Cox, N. L. J., Cami, J., Kaper, L., et al. 2014, *A&A*, **569**, A117
 Donati, J.-F. 2003, in ASP Conf. Ser. 307, *Solar Polarization*, ed. J. Trujillo-Bueno & J. Sanchez Almeida (San Francisco: ASP), 41

Foing, B. H., & Ehrenfreund, P. 1994, [Natur](#), **369**, 296
Foing, B. H., & Ehrenfreund, P. 1997, [A&A](#), **317**, L59
Fulara, J., Jakobi, M., & Maier, J. P. 1993, [CPL](#), **211**, 227
Hiltner, W. A. 1956, [ApJS](#), **2**, 389

Martoli, E., Teeple, D., Manset, N., et al. 2012, [Proc. SPIE](#), **8451**, 2
Walker, G. A. H. 1962, [MNRAS](#), **125**, 141
Walker, G. A. H., Bohlender, D. A., Maier, J. P., & Campbell, E. K. 2015, [ApJL](#), **812**, L8